

This document contains a post-print version of the paper

## Motion planning for an adaptive wing structure with Macro-fiber Composite actuators

authored by **J. Schröck, T. Meurer, and A. Kugi**

and published in *SPIE Europe: Microtechnologies for the New Millennium, Smart Sensors, Actuators, and MEMS IV*.

---

The content of this post-print version is identical to the published paper but without the publisher's final layout or copy editing. Please, scroll down for the article.

---

### Cite this article as:

J. Schröck, T. Meurer, and A. Kugi, "Motion planning for an adaptive wing structure with macro-fiber composite actuators", in *SPIE Europe: Microtechnologies for the New Millennium, Smart Sensors, Actuators, and MEMS IV*, Dresden, Germany, Apr. 2009. DOI: [10.1117/12.821699](https://doi.org/10.1117/12.821699)

---

### BibTex entry:

```
@inproceedings{Schrock09b,  
  author = {Schröck, J. and Meurer, T. and Kugi, A.},  
  title = {Motion planning for an adaptive wing structure with Macro-fiber Composite actuators},  
  booktitle = {SPIE Europe: Microtechnologies for the New Millennium, Smart Sensors, Actuators, and MEMS IV  
  },  
  month = {04.05.},  
  year = {2009},  
  address = {Dresden, Germany},  
  doi = {10.1117/12.821699}  
}
```

---

### Link to original paper:

<http://dx.doi.org/10.1117/12.821699>

---

### Read more ACIN papers or get this document:

<http://www.acin.tuwien.ac.at/literature>

---

### Contact:

Automation and Control Institute (ACIN)  
Vienna University of Technology  
Gusshausstrasse 27-29/E376  
1040 Vienna, Austria

Internet: [www.acin.tuwien.ac.at](http://www.acin.tuwien.ac.at)  
E-mail: [office@acin.tuwien.ac.at](mailto:office@acin.tuwien.ac.at)  
Phone: +43 1 58801 37601  
Fax: +43 1 58801 37699

---

### Copyright notice:

Copyright 2009 Society of Photo-Optical Instrumentation Engineers. One print or electronic copy may be made for personal use only. Systematic reproduction and distribution, duplication of any material in this paper for a fee or for commercial purposes, or modification of the content of the paper are prohibited.  
<http://dx.doi.org/10.1117/12.821699>

# Motion Planning for an Adaptive Wing Structure with Macro-fiber Composite Actuators

J. Schröck, T. Meurer, and A. Kugi

Automation and Control Institute, Vienna University of Technology,  
Gußhausstr. 27–29, 1040 Vienna, Austria

## ABSTRACT

A systematic approach for flatness-based motion planning and feedforward control is presented for the transient shaping of a piezo-actuated rectangular cantilevered plate modeling an adaptive wing. In the first step the consideration of an idealized infinite-dimensional input allows to determine the state and input parametrization in terms of a flat or basic output, which is used for a systematic motion planning approach. Subsequently, the obtained idealized input function is projected onto a finite number of suitably placed Macro-fiber Composite (MFC) patch actuators. The tracking performance of the proposed approach is evaluated in a simulation scenario.

**Keywords:** Trajectory planning, feedforward control, cantilever plate, tracking, flatness

## 1. INTRODUCTION

Smart structures nowadays can be found in a large variety of applications with vibration suppression in lightweight structures representing one of the classical key examples. Due to the vast progress in both material as well as actuator development new application areas evolve such as adaptive optics in telescopes, adaptive wings, or so-called smart skins, see, e.g., Ref. 1. Here it is desired to suitably affect the shape of a structure in order to achieve, e.g., the modulation of optical wave fronts, the reduction of drag, or the improvement of aeroelastic characteristics. Thereby, piezoelectric elements typically serve as actuators by exploiting the indirect piezoelectric effect, which allows to convert electrical voltage into mechanical strain.

For flexible structures, in general two problems have to be distinguished. In the so-called static or dynamic shape control, the undeformed or respectively the initial state of a structure is preserved in view of static or dynamic disturbances (see, e.g., Ref. 2 for a comprehensive overview). On the other hand, the transient shaping of a flexible structure, i.e. the design of a suitable input in order to achieve a transient change of the structural shape, provides new and particularly promising applications. This is for example outlined in Ref. 3 for a piezo-actuated simply-supported elastic plate. There, flatness-based methods (see, e.g., Ref. 4–6) for motion planning and feedforward control design are combined with results from optimal actuator placement to achieve a desired transient shaping of the plate.

In the following, these results are extended to realize the transient shaping of a cantilevered Kirchhoff plate by piezoelectric actuation. This configuration for example represents a simple model of an adaptive wing with the wing shape changing transiently according to an appropriately prescribed desired wing profile. For this, in a first step an idealized setting is considered, where the input acts arbitrarily on the plate, which directly allows a parametrization of the deflection and the input in terms of a flat or basic output and its spatial and temporal derivatives. This inverse system representation can be efficiently utilized for motion planning, namely the determination of a suitable transient deflection profile, e.g., a flapping wing motion. In a second step the idealized setting is projected to a realistic one where the input acts via suitably located piezo actuators. In this scenario Macro-fiber Composite (MFC) patch actuators are considered, which provide high flexibility and a larger piezoelectric coupling coefficient than monolithic piezoceramic (PZT) patches. The presented patch configuration is determined by maximizing the controllability gramians of the the first two eigenmodes for motion planning while minimizing the control spillover.

---

Further author information: (Send correspondence to J.S.)

J.S.: E-mail: schroeck@acin.tuwien.ac.at, Telephone: +43 1 58801 37625

T.M.: E-mail: meurer@acin.tuwien.ac.at, Telephone: +43 1 58801 37627

A.K.: E-mail: kugi@acin.tuwien.ac.at, Telephone: +43 1 58801 37600

The paper is organized as follows: in Section 2, the equations of motion for the MFC-actuated plate are determined using Hamilton's principle. Based on the corresponding variational formulation and spectral analysis in Section 3, motion planning and feedforward control design for the plate are considered in Section 4. Simulation results for the controlled bending and torsion motion of an airfoil are presented in Section 5.

## 2. MODELING OF THE MFC-ACTUATED CANTILEVERED KIRCHHOFF PLATE

In the following, a cantilevered rectangular isotropic Kirchhoff plate is considered, which is actuated by a finite number of MFC-patches that are symmetrically placed on the upper and lower surface of the plate. For the derivation of the governing equations let  $\mathcal{B} = \{e_1, e_2, e_3\}$  denote the orthonormal basis of a three-dimensional Euclidean space with coordinates  $x^j$ ,  $j = 1, 2, 3$ . Assuming small displacements of a thin plate, homogeneous and isotropic material, neglecting transverse shear effects, and assuming that linear filaments of the plate initially perpendicular to the middle surface remain straight and perpendicular to the deformed middle surface without undergoing tension or contraction (Kirchhoff assumption), the potential energy due to bending reads as

$$W_p = \frac{1}{2} D_E \int_{\Omega} \left[ (\nabla^2 w)^2 + 2(1-\nu) \left( \left( \frac{\partial^2 w}{\partial(x^1)\partial(x^2)} \right)^2 - \frac{\partial^2 w}{\partial(x^1)^2} \frac{\partial^2 w}{\partial(x^2)^2} \right) \right] dx^1 dx^2. \quad (1)$$

Here,  $\Omega$  represents the plate domain  $\Omega = (0, L_1) \times (0, L_2)$ ,  $w(\underline{x}, t) = w(x^1, x^2, t)$  denotes the plate deflection in the  $x^3$ -direction,  $\nabla^2 = \partial^2/\partial(x^1)^2 + \partial^2/\partial(x^2)^2$ , and  $D_E = EH^3/(12(1-\nu^2))$  yields the flexural rigidity with Young's modulus  $E$ , Poisson's ratio  $\nu$ , and the plate height  $H$ . Neglecting the rotational inertia of the plate, its kinetic energy due to bending follows as

$$W_k = \frac{1}{2} \int_{\Omega} \rho H \left( \frac{\partial w}{\partial t} \right)^2 dx^1 dx^2 \quad (2)$$

with  $\rho$  the mass density of the plate.

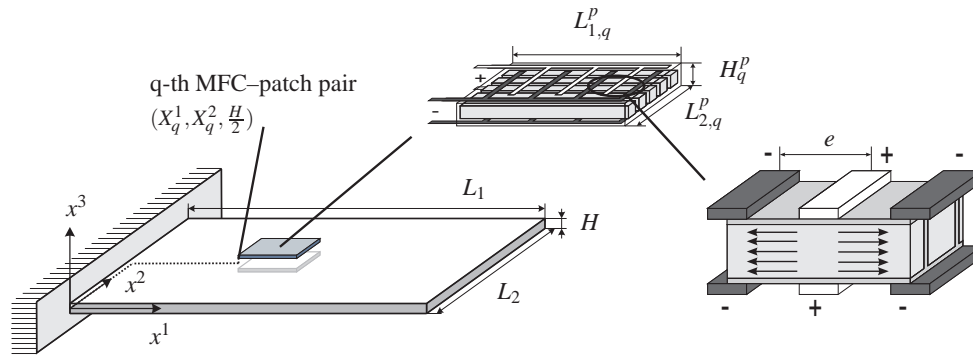


Figure 1. Schematics of the considered MFC-actuated cantilevered plate with details on the structure of an MFC-patch.

MFC-patch actuators are composed of rectangular piezoceramic fibers embedded in an epoxy matrix which are covered by interdigitated electrodes on both sides (cf. Fig. 1). For modeling purposes this complex structure is replaced by a homogenized orthotropic material with appropriate material parameters provided by the distributor, see Ref. 7. While the kinetic energy of the actuators is neglected the potential energy of an MFC-patch at time  $t$  is given in the form

$$W_{pa} = \int_0^t \int_V \left( \sigma^{ij} \frac{\partial}{\partial \tau} \varepsilon_{ij} + E_i \frac{\partial}{\partial \tau} D^i \right) dx^1 dx^2 dx^3 d\tau, \quad (3)$$

with the mechanical stress  $\sigma$ , the strain  $\varepsilon$ , the electric field  $E$ , the electric flux density  $D$  and  $V$  as the volume of the MFC-patch. By consideration of the general constitutive relations of piezoelectric material, see, e.g., Ref. 8

$$\begin{aligned} \sigma^{ij} &= c^{ijkl} \varepsilon_{kl} - h_m^{ij} D^m, \\ E_n &= -h_n^{kl} \varepsilon_{kl} + \beta_{nm} D^m, \end{aligned} \quad (4)$$

with the integrability conditions

$$c^{ijkl} = c^{jikl} = c^{jilk} = c^{klij}, \quad h_m^{kl} = h_m^{lk}, \quad \beta_{nm} = \beta_{mn}, \quad (5)$$

the potential energy (3) evaluates to

$$W_{pa} = \frac{1}{2} \int_V \left( c^{ijkl} \varepsilon_{ij} \varepsilon_{kl} - 2h_m^{ij} D^m \varepsilon_{ij} + \beta_{nm} D^n D^m \right) dx^1 dx^2 dx^3. \quad (6)$$

In the following the electric field between the interdigitated electrodes in the MFC-patch is approximated by an exclusive homogeneous field component  $E_1$  (cf. Fig. 1). Due to the Kirchhoff assumption of zero traverse strains,  $\varepsilon_{33} = \varepsilon_{13} = \varepsilon_{23} = 0$  the shear stresses in  $x^3$ -direction for orthotropic material disappear  $\sigma^{23} = \sigma^{13} = 0$ . On the additional assumption of a zero traverse stress component  $\sigma^{33} = 0$  and of vanishing electric flux density components  $D^2 = D^3 = 0$  the constitutive relations (4) simplify to

$$\begin{aligned} \begin{bmatrix} \sigma^{11} \\ \sigma^{22} \\ \sigma^{12} \end{bmatrix} &= \begin{bmatrix} c^{1111} & c^{1122} & 0 \\ c^{2211} & c^{2222} & 0 \\ 0 & 0 & c^{1212} \end{bmatrix} \begin{bmatrix} \varepsilon_{11} \\ \varepsilon_{22} \\ \varepsilon_{12} \end{bmatrix} - \begin{bmatrix} h_1^{11} \\ h_1^{22} \\ 0 \end{bmatrix} D^1, \\ E_1 &= \begin{bmatrix} -h_1^{11} & -h_1^{22} & 0 \end{bmatrix} \begin{bmatrix} \varepsilon_{11} \\ \varepsilon_{22} \\ \varepsilon_{12} \end{bmatrix} + \beta_{11} D^1. \end{aligned} \quad (7)$$

Note that the material parameter  $h_1^{12} = 0$  in this case. Assuming that the self-generated electric field due to the direct piezoelectric effect  $-h_i^{ii} \varepsilon_{ii}$  with  $i \in \{1, 2\}$  is insignificant compared to the field component  $E_1$  the integration along  $E_1$  between two neighboring electrodes spaced by the distance  $e$  leads to

$$\int_{x_e}^{x_e+e} E_1 dx^1 = \beta_{11} D^1 e = U, \quad (8)$$

where  $U$  denotes the voltage applied to actuator. Hence, if the stiffness of the MFC-patch actuator  $c^{ijkl}$  is neglected and the voltage sources are considered to be ideal such that the term  $\beta_{nm} D^n D^m$  vanishes in the following variation formulation the potential energy (6) reads as

$$W_{pa} = \gamma^p U \int_{\Omega^p} \left( \frac{h_1^{11}}{\beta_{11}} \frac{\partial^2 w}{\partial (x^1)^2} + \frac{h_1^{22}}{\beta_{11}} \frac{\partial^2 w}{\partial (x^2)^2} \right) dx^1 dx^2, \quad (9)$$

with  $\gamma^p = H^p(H + H^p)/(2e)$ ,  $H_p$  the patch height and  $\Omega^p$  the plate area covered by the patch. In order to induce bending of the plate each actuator pair is driven in an asymmetric configuration with the voltage applied to the upper and lower electrodes given by  $U^u(t) = U_0 + U(t)$ , and  $U^l(t) = U_0 - U(t)$ , respectively, where  $U_0$  denotes a constant supply voltage to symmetrically preload the MFC actuators. With this specific voltage control the potential energy of an MFC-patch pair is equal to the energy given in (9) multiplied by a factor 2.

With these preparations, the equations of motion of the MFC-actuated plate can be directly determined using Hamilton's principle, which yields the strong formulation of the considered system for  $(\underline{x}, t) \in \Omega \times \mathbb{R}^+$  in form of

$$\rho H \frac{\partial^2 w}{\partial t^2} + D_E \nabla^4 w + u = 0, \quad (10)$$

see also Ref. 9, where  $\nabla^4 = \frac{\partial^4}{\partial (x^1)^4} + 2 \frac{\partial^4}{\partial (x^1)^2 \partial (x^2)^2} + \frac{\partial^4}{\partial (x^2)^4}$  is known as the bi-harmonic operator and

$$u(\underline{x}, t) = 2 \sum_{q=1}^m \gamma_q^p U_q(t) \left( \frac{h_1^{11}}{\beta_{11}} \frac{\partial^2}{\partial (x^1)^2} \Lambda_q(\underline{x}) + \frac{h_1^{22}}{\beta_{11}} \frac{\partial^2}{\partial (x^2)^2} \Lambda_q(\underline{x}) \right) \quad (11)$$

represents the effect of the  $m \geq 1$  attached pairs of MFC-patches with spatial characteristics  $\Lambda_q(\underline{x})$ . For the cantilevered plate, the respective boundary conditions (BCs) follow as

$$w = 0, \quad \frac{\partial w}{\partial (x^1)} = 0, \quad \text{for } x^1 = 0 \quad (12)$$

$$\left. \begin{aligned} \frac{\partial^2 w}{\partial y^2} + \nu \frac{\partial^2 w}{\partial s^2} &= 0, \\ \frac{\partial^3 w}{\partial n^3} + (2 - \nu) \frac{\partial^3 w}{\partial n \partial s^2} &= 0 \end{aligned} \right\} \quad \text{for } x^1 = L_1 \vee x^2 = 0 \vee x^2 = L_2, \quad (13)$$

where  $n$  and  $s$  denote the normal and the tangent component to the respective boundary, e.g.  $n = x^1$  and  $s = x^2$  at  $x^1 = L_1$ .

For the sake of simplicity, zero initial conditions (ICs) are assumed, which for stationary ICs can be obtained by a simple state transformation. Furthermore, it should be pointed out that gravitational effects can be easily incorporated by adding the term  $\int_{\Omega} \rho g H w dx^1 dx^2$  to the potential energy (1) with the gravitational constant  $g$ .

### 3. VARIATIONAL FORMULATION AND SPECTRAL ANALYSIS

From (11) it follows that any spatial patch characteristics  $\Lambda_q(\underline{x})$  has to be twice continuously differentiable. Hence, for piezoelectric patches with spatial characteristics of the form (cf. Fig. 1)

$$\Lambda_q(\underline{x}) = \left[ h(x^1 - X_q^1) - h(x^1 - X_q^1 - L_{1,q}^p) \right] \times \left[ h(x^2 - X_q^2) - h(x^2 - X_q^2 - L_{2,q}^p) \right], \quad (14)$$

where  $h(\cdot)$  denotes the Heaviside function, it is required to consider the weak or variational form, see, e.g., Ref. 10, of (10)-(13) for a suitable class of test functions  $\xi(\underline{x})$ .

#### 3.1 Weak and Variational Formulation

Let  $\mathcal{V} = H_{\Gamma_0}^2(\Omega)$  where  $\Gamma_0 = \{\underline{x} \mid x^1 = 0\}$  and let  $\mathcal{H} = L^2(\Omega)$ . Given  $\xi(\underline{x}) \in \mathcal{V}$  the weak form of (10)-(13) follows directly from the determined energies, i.e.

$$\int_{\Omega} \rho H \frac{\partial^2 w}{\partial t^2} \xi dx^1 dx^2 + a(w, \xi) = -2 \sum_{q=1}^m \gamma_q^p U_q(t) \int_{\Omega_q^p} \left( \frac{h_1^{11}}{\beta_{11}} \frac{\partial^2 \xi}{\partial (x^1)^2} + \frac{h_1^{22}}{\beta_{11}} \frac{\partial^2 \xi}{\partial (x^2)^2} \right) dx^1 dx^2 \quad (15)$$

with

$$a(w, \xi) = D_E \int_{\Omega} \left[ \left( \frac{\partial^2 w}{\partial (x^1)^2} + \nu \frac{\partial^2 w}{\partial (x^2)^2} \right) \left( \frac{\partial^2 \xi}{\partial (x^1)^2} + \nu \frac{\partial^2 \xi}{\partial (x^2)^2} \right) + (1 - \nu^2) \frac{\partial^2 w}{\partial (x^1)^2} \frac{\partial^2 \xi}{\partial (x^2)^2} + 2(1 - \nu) \frac{\partial^2 w}{\partial (x^1) \partial (x^2)} \frac{\partial^2 \xi}{\partial (x^1) \partial (x^2)} \right] dx^1 dx^2 \quad (16)$$

such that  $W_p = a(w, w)/2$ . The existence and uniqueness of the solution  $w(\cdot, t) \in \mathcal{V}$  can be established by considering (15) in the dual space  $\mathcal{V}^*$  as shown in Ref. 10. In the following, only the results are summarized, which are essential for the further analysis.

Note that (16) represents a sesquilinear form for all  $w, \xi \in \mathcal{V}$  with  $a(w, w) \geq 0$  and  $a(w, w) = 0$  iff  $w = 0$ . In addition, the spaces  $\mathcal{V}$  and  $\mathcal{H}$  form a Gelfand triple  $\mathcal{V} \subset \mathcal{H} \simeq \mathcal{H}^* \subset \mathcal{V}^*$ , where  $\mathcal{H}$  can be identified with its dual  $\mathcal{H}^*$  by the Riesz representation theorem. Hence, the duality pairing  $\langle F, \xi \rangle_{\mathcal{V}^*, \mathcal{V}} = F(\xi)$  with  $F \in \mathcal{V}^*$ ,  $\xi \in \mathcal{V}$  can be considered as the continuous extension of the inner product  $\langle \cdot, \cdot \rangle_{\mathcal{H}}$  on  $\mathcal{V}^* \times \mathcal{V}$ . Defining  $u$  from (11) as  $u \in \mathcal{V}^*$  by

$$\langle u, \xi \rangle_{\mathcal{V}^*, \mathcal{V}} = \left\langle 2 \sum_{q=1}^m \gamma_q^p U_q(t) \Lambda_q(\underline{x}), \frac{h_1^{11}}{\beta_{11}} \frac{\partial^2 \xi}{\partial (x^1)^2} + \frac{h_1^{22}}{\beta_{11}} \frac{\partial^2 \xi}{\partial (x^2)^2} \right\rangle_{\mathcal{H}}, \quad (17)$$

the weak form (15) can be formulated as

$$\left\langle \rho H \frac{\partial^2 w}{\partial t^2}, \xi \right\rangle_{\mathcal{V}^*, \mathcal{V}} + a(w, \xi) = \left\langle -2 \sum_{q=1}^m \gamma_q^p U_q(t) \left( \frac{h_1^{11}}{\beta_{11}} \frac{\partial^2}{\partial (x^1)^2} \Lambda_q(\underline{x}) + \frac{h_1^{22}}{\beta_{11}} \frac{\partial^2}{\partial (x^2)^2} \Lambda_q(\underline{x}) \right), \xi \right\rangle_{\mathcal{V}^*, \mathcal{V}}. \quad (18)$$

Note that for control design, (18) can be re-written as an abstract first order differential equation in the product space  $\mathcal{V} \times \mathcal{H}$ , see Ref. 10. On the other hand, the variational formulation is particularly suitable to determine a spectral representation of the system dynamics by selecting the test function  $\xi(\underline{x})$  from the orthonormal set of eigenfunctions of the bi-harmonic operator  $\nabla^4$ .

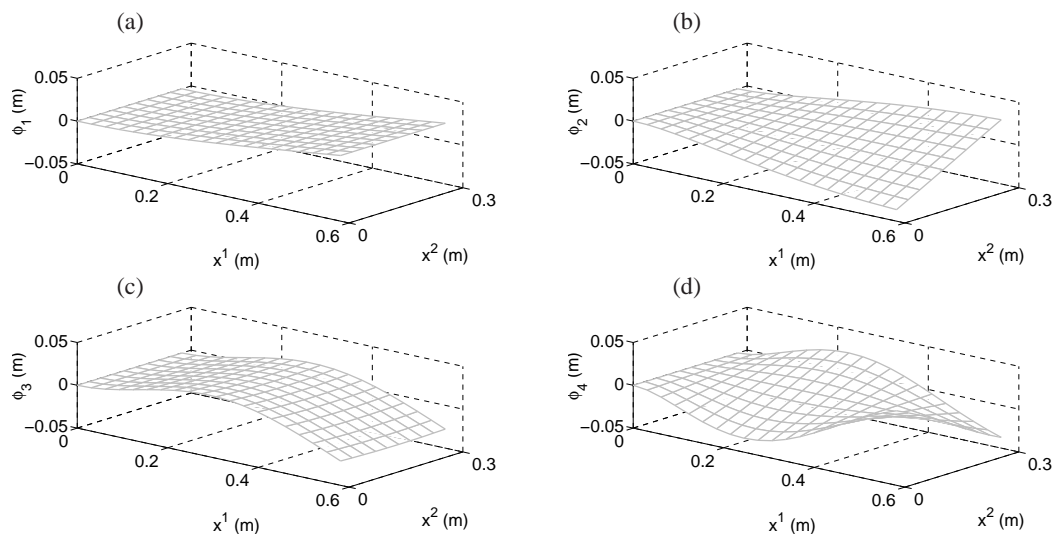


Figure 2. Orthonormalized eigenfunctions  $\phi_k(\underline{x})$  for  $k \in \{1, 2, 3, 4\}$ .

### 3.2 Eigenproblem for the Cantilevered Plate

Consider the bi-harmonic operator

$$A\phi = \nabla^4 \phi$$

defined on the domain

$$\mathcal{D}(A) = \left\{ \phi \in H_{\Gamma_0}^4(\Omega) \mid \frac{\partial^2 \phi}{\partial n^2} + \nu \frac{\partial^2 \phi}{\partial s^2} = 0, \frac{\partial^3 \phi}{\partial n^3} + (2 - \nu) \frac{\partial^3 \phi}{\partial n \partial s^2} = 0 \text{ at } x^1 = L_1 \vee x^2 = 0 \vee x^2 = L_2 \right\}. \quad (19)$$

In particular,  $A : \mathcal{D}(A) \subset \mathcal{V} \rightarrow \mathcal{V}$  is a linear self-adjoint operator with domain dense in  $\mathcal{V}$ . Furthermore, the eigenproblem

$$A\phi = \lambda \phi, \quad \phi \in \mathcal{D}(A) \quad (20)$$

admits a sequence of real eigenvalues  $\{\lambda_k\}_{k \in \mathbb{N}}$  of finite multiplicity satisfying

$$0 < \lambda_1 \leq \lambda_2 \leq \dots \leq \lambda_n \leq \dots \rightarrow \infty.$$

The respective eigenfunctions  $\{\phi_k(\underline{x})\}_{k \in \mathbb{N}}$  (cf. Fig. 2) form an orthonormal basis for  $\mathcal{V}$  such that  $A$  can be represented as  $Aw = \sum_{k \in \mathbb{N}} \lambda_k \langle w, \phi_k \rangle \phi_k$  for any  $w \in \mathcal{D}(A)$  with  $\mathcal{D}(A) = \{w \in \mathcal{V} \mid \sum_{k \in \mathbb{N}} |\lambda_k|^2 |\langle w, \phi_k \rangle|^2 < \infty\}$ , see, e.g., Ref. 11. Note that exact solutions to the eigenproblem (20) are not available for the considered clamped-free case. In order to determine approximate solutions, typically a Rayleigh-Ritz approach is applied with ansatz functions constructed from the set of eigenfunctions for a cantilevered beam (in the  $x^1$ -direction) and a beam with both ends free (in the  $x^2$ -direction), see, e.g., Ref. 12. This allows to obtain a rather high accuracy in the approximation of the eigenvalues. However, the determined ansatz functions do not satisfy the natural BCs (13), which results in a rather poor convergence of the ansatz functions to the eigenfunctions of the plate. Since the proposed approach for motion planning relies on both the eigenvalues and the eigenfunctions, for the results presented in the following a high-order finite-difference discretization is applied to calculate an approximate solution to the eigenproblem (20), which satisfies the clamped-free BCs at the respective grid points. Note that this approach also allows to incorporate additional effects such as the local stiffening of the structure due to the attached MFC-patches, which are neglected in this contribution.

### 3.3 Spectral Representation

With the results of the previous section, the spectral or modal representation of the MFC-actuated plate equation can be determined by considering the series expansion

$$w = \sum_{k \in \mathbb{N}} w_k \phi_k \quad (21)$$

with the  $k$ -th modal state  $w_k(t)$  and the eigenfunction  $\phi_k(\underline{x})$ . Substitution of (21) into the weak or the variational formulation (15) or (18), respectively, and choosing the test function  $\xi(\underline{x}) = \phi_k(\underline{x})$  for fixed but arbitrary  $k \in \mathbb{N}$  yields the modal representation

$$\frac{d^2 w_k}{dt^2} = -\omega_k^2 w_k - 2 \sum_{q=1}^m U_q(t) \frac{\gamma_q^p}{\rho H} \int_{\Omega_q^p} \left( \frac{h_1^{11}}{\beta_{11}} \frac{\partial^2}{\partial (x^1)^2} \phi_k + \frac{h_1^{22}}{\beta_{11}} \frac{\partial^2}{\partial (x^2)^2} \phi_k \right) dx^1 dx^2, \quad (22)$$

where  $\omega_k^2 = D_E \lambda_k / (\rho H)$  denotes the  $k$ -th eigenfrequency. This result follows in a straightforward manner by applying Green's theorem together with (20) and the fact that  $\phi_k(\underline{x}) \in \mathcal{D}(A) \subset \mathcal{V}$  with  $\langle \phi_k, \phi_l \rangle_{\mathcal{H}} = \delta_{k,l}$  for all  $k, l \in \mathbb{N}$  with the Kronecker symbol  $\delta_{k,l}$ .

In the following, both the strong (10)-(13) and the modal representation (22) for the MFC-actuated Kirchhoff plate are utilized for motion planning and feedforward tracking control design.

## 4. MOTION PLANNING FOR THE PIEZO-ACTUATED CANTILEVERED PLATE

In order to determine the input voltages  $U_q(t)$ ,  $q = 1, \dots, m$  to the attached pairs of MFC-patches, which are required to realize a prescribed transient shaping of the plate, in a first step an idealized scenario is considered under the assumption of an infinite-dimensional input  $u(\underline{x}, t)$  acting arbitrarily on the domain  $\Omega$ . This enables to introduce a flat or basic output, which provides an easily applicable approach for motion planning. For the realization of the determined motion, in a second step, the determined  $u(\underline{x}, t)$  is projected onto a finite number of suitably placed MFC-patches by using results from optimal actuator placement.

### 4.1 Idealized Flatness-based Parametrization

Let the number of MFC-patch pairs  $m \rightarrow \infty$  while simultaneously each  $\Omega_q^p \rightarrow 0$ ,  $q = 1, \dots, m$ . In this case,  $u(\underline{x}, t)$  as defined in (11) represents a distributed input acting arbitrarily on the domain  $\Omega$ . Under this assumption, let  $y(\underline{x}, t) = w(\underline{x}, t)$ , which in view of (10), (11) directly provides the inverse system representation in terms of  $y(\underline{x}, t)$  and its spatial and time-derivatives, i.e.

$$w = y \quad (23)$$

$$u = - \left( \rho H \frac{\partial^2 y}{\partial t^2} + D_E \nabla^4 y \right). \quad (24)$$

Hence, prescribing suitable trajectories  $(\underline{x}, t) \mapsto y^d(\underline{x}, t)$  for the basic output satisfying the BCs (12), (13), i.e.  $y^d(\underline{x}, t) \in C^2(\Xi; \mathcal{D}(A))$  for  $\Xi \subset \mathbb{R}^+$ , the evaluation of (24) directly yields the feedforward control  $u^d(\underline{x}, t)$ , which is required to track the deflection profile  $w^d(\underline{x}, t) = y^d(\underline{x}, t)$  in open-loop. Obviously, for the considered idealized scenario with an input acting arbitrarily on the plate domain  $\Omega$ , an inversion-based solution to the tracking control problem follows naturally from the governing PDE. Prior to discussing the implications of the considered idealization in view of the realization of  $u^d(\underline{x}, t)$  by a finite number of MFC-patches, the problem of motion planning, i.e. the choice of suitable  $y^d(\underline{x}, t) \in C^2(\Xi; \mathcal{D}(A))$ , is considered.

### 4.2 Motion Planning

Since the eigenfunctions  $\phi_k(\underline{x})$ ,  $k \in \mathbb{N}$  satisfy  $\phi_k(\underline{x}) \in \mathcal{D}(A)$ , it follows directly that the choice

$$y^d = \sum_{k \in I_n} a_k \phi_k \quad (25)$$

with time-varying coefficients  $a_k(t) \in C^2(\Xi)$  for an  $n$ -dimensional index set  $I_n \subset \mathbb{N}$  ensures that  $y^d(\underline{x}, t) \in C^2(\Xi; \mathcal{D}(A))$ . Hence, re-planning  $a_k(t)$ ,  $k \in I_n$  yields different deflection profiles  $w^d(\underline{x}, t) = y^d(\underline{x}, t)$ . As an example, in Ref. 3 the determination of a desired profile is considered in order to achieve a transient deflection of a simply-supported plate realizing the formation of a bulge whose global minimum moves along a prescribed path in the  $(x^1, x^2)$ -plane.

In the following, the bending and torsional motion of an airfoil is considered by a prescribed time-varying superposition of the first two eigenfunctions  $\phi_k(\underline{x})$ ,  $k \in I_2 = \{1, 2\}$ , which are depicted in Fig. 2 (a),(b). Note that more general trajectories can be treated similarly. In particular, the coefficients  $a_k(t)$ ,  $k \in I_2$  in (25) are chosen as

$$a_k(t) = A_k \left( g_{\sigma_k, T_k^0}(t - t_k^0) - g_{\sigma_k, T_k^1}(t - t_k^1) \right) \quad (26)$$

where

$$g_{\sigma, T}(t) = \begin{cases} 0 & t \leq 0 \\ 1 & t \geq T \\ \frac{\int_0^t h_{\sigma, T}(\tau) d\tau}{\int_0^T h_{\sigma, T}(\tau) d\tau} & t \in (0, T), \end{cases} \quad (27)$$

with

$$h_{\sigma, T}(t) = \begin{cases} 0 & t \notin (0, T) \\ \exp\left(\frac{-1}{(1-\frac{t}{T})^\sigma}\right) & t \in (0, T). \end{cases}$$

The parameters  $T_k^j$ ,  $j = 0, 1$  and  $t_k^0 < t_k^1$ ,  $k \in I_2$  are chosen such that the desired profile  $y^d(\underline{x}, t)$  as defined in (25) realizes the transition from the initial profile  $y^d(\underline{x}, 0) = 0$  to the first profile  $y^d(\underline{x}, t_1^0 + T_1^0) = a_1 \phi_1(\underline{x})$  (cf. Fig. 2 (a)) followed by the transition to the final profile  $y^d(\underline{x}, t_2^0 + T_2^0) = a_2 \phi_2(\underline{x})$  (cf. Fig. 2 (b)). Obviously, the question arises whether the corresponding idealized infinite-dimensional input  $u^d(\underline{x}, t)$  resulting from the substitution of  $y^d(\underline{x}, t)$  into (24) can be projected onto a finite number of inputs in order to accurately realize the desired motion  $w^d(\underline{x}, t) = y^d(\underline{x}, t)$ . As is illustrated in the following, this results in an approximate feedforward tracking control, which utilizes the spectral system representation (22) in combination with a suitable optimization-based approach for the distribution of a certain number of MFC-patches.

### 4.3 Approximate Flatness-based Parametrization

For the realization of the determined idealized feedforward control, recall that from (24) and the ansatz for the desired trajectory (25),  $u^d(\underline{x}, t)$  evaluates to

$$u^d = - \sum_{k \in I_n} \left[ \rho H \frac{d^2 a_k(t)}{dt^2} + D_E \lambda_k a_k(t) \right] \phi_k$$

since  $\nabla^4 \phi_k(\underline{x}) = \lambda_k \phi_k(\underline{x})$  by (20). Hence, the coefficients  $u_k^d(t)$  of  $u^d(\underline{x}, t)$  with respect to the basis  $\{\phi_k(\underline{x})\}_\gamma$  read as

$$u_k^d = \begin{cases} - \left( \rho H \frac{d^2 a_k(t)}{dt^2} + D_E \lambda_k a_k(t) \right), & k \in I_n \\ 0, & k \in \mathbb{N} \setminus I_n. \end{cases} \quad (28)$$

As expected from the motion planning approach of the previous section, in the modal representation only the  $n$  modal states  $w_k(t)$ ,  $k \in I_n$  are excited by the feedforward control. In view of the modal representation (22), this directly implies that  $m \geq n$  pairs of MFC-patches are required for the realization of the desired profile. Moreover, the conditions

$$2 \sum_{q=1}^m U_q(t) \gamma_q^p \int_{\Omega_q^p} \left( \frac{h_1^{11}}{\beta_{11}} \frac{\partial^2}{\partial (x^1)^2} \phi_k + \frac{h_1^{22}}{\beta_{11}} \frac{\partial^2}{\partial (x^2)^2} \phi_k \right) dx^1 dx^2 = \begin{cases} u_k^d, & k \in I_n \\ 0, & k \in \mathbb{N} \setminus I_n \end{cases} \quad (29)$$

have to be satisfied, which relate the spectral representations of the idealized input  $u_k^d(t)$  given by (28) and the actuation of the  $m$  pairs of MFC-patches as introduced in (22).

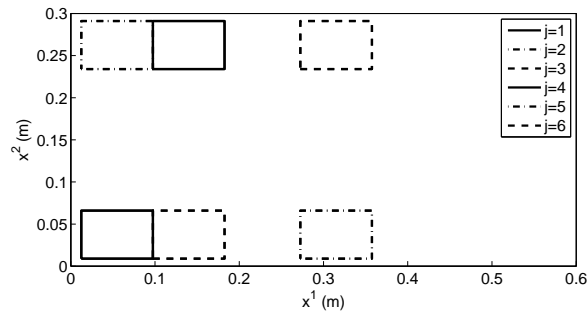


Figure 3. Actuator configuration for  $m = 6$  MFC-patches for the realization of the desired trajectory (25) with coefficients (26).

The conditions (29) constitute a linear system of equations for the input voltages  $U_q(t)$ ,  $q = 1, \dots, m \geq n$ . It is obvious that only  $m$  equations can be solved while the remaining (infinite) homogeneous equations not necessarily evaluate to zero. This corresponds to the well-known control spillover, i.e. the excitation of modes not considered for control design, which might decrease the achievable tracking performance. Hence, only an approximate realization of the idealized flatness-based feedforward tracking control is possible. However, it can be directly deduced from the left hand side of (29) that the size, shape, and location of the MFC-patches serves as degrees-of-freedom, which can be efficiently utilized twofold. At first a suitable shaping and placement allows to decrease the control effort, i.e. the necessary amplitudes of the input voltages  $U_q(t)$ ,  $q = 1, \dots, m$ , which are required to excite the modes  $w_k(t)$ ,  $k \in I_n$  considered for motion planning. Secondly, it is possible to significantly reduce the control spillover.

#### 4.4 Realization by Optimal Actuator Placement

In general, the available results for the optimal placement of actuators and sensors for flexible structures are based on a modal system representation according to (22). Thereby the use of controllability gramians, see, e.g., Ref. 13 or spatial  $H^2$ -norms Ref. 14 is proposed in order to improve a certain controllability measure while minimizing the effect of residual modes. However, besides the fact that in particular the latter criterion performs best if each MFC-patch is placed independently by neglecting the interactions of multiple actuators, the focus of these approaches is rather related to vibration suppression than to tracking control with the desire to transiently shape a given structure. Additionally possible actuator limitations have to be taken into account, i.e. in the case of piezoelectric patches that the applicable input voltage is limited. Hence, the appropriate location and shape of the patches is of crucial importance in view of applications.

For the realization of the combined bending and torsional motion as introduced in (26), at least 2 pairs of patches are required. In order to deal with the voltage limitations as well as control spillover, in the following, six quadratic patch pairs are distributed on the plate according to Fig. 3. The patch location was thereby determined by maximizing the controllability gramians of the first two modes  $w_k(t)$ ,  $k = 1, 2$  considered for motion planning while minimizing the control spillover. Once the patch distribution is determined, the corresponding voltages  $U_q(t)$ ,  $q = 1, \dots, 6$  are directly obtained by solving (29). However, the combinatorial complexity arising from the available degrees-of-freedom, i.e. shape, location, and orientation of the patches, requires the incorporation of an appropriate optimization approach in view of the demands of motion planning, which is a topic of current research.

### 5. SIMULATION RESULTS

For the numerical simulation, a rectangular plate of dimension  $L_1 = 0.6$  m,  $L_2 = 0.3$  m, and  $H = 1 \times 10^{-3}$  m is considered with the material properties  $\rho = 1800$  kg/m<sup>3</sup>,  $E = 20$  GPa, and  $\nu = 0.33$  corresponding to a fiber re-enforced composite. The actuator configuration is depicted in Fig. 3, which includes  $m = 6$  pairs of MFC-patches. The dimensions of the patches correspond to  $L_{1,q}^p = 0.085$  m,  $L_{2,q}^p = 0.057$  m,  $H_p = 3 \times 10^{-4}$  m and the material parameters according to Ref. 7 are given by  $\gamma_q^p = 2.55 \times 10^{-4}$  m,  $h_1^{11}/\beta_{11} = 13.61$  N/m/V,  $h_1^{22}/\beta_{11} = -1.12$  N/m/V with  $q = 1, \dots, 6$ . Note that anisotropic material behavior as well as the local stiffening of the structure by the attached MFC-patches are subsequently neglected. However, as already pointed out above, these effects only influence the considered eigenproblem and can be easily incorporated into the analysis. The prescribed bending and torsional motion as defined in (25), (26) is parametrized by  $a_1 = 6.4 \times 10^{-3}$  m,  $a_2 = 2.4 \times 10^{-3}$  m,  $t_1^0 = 0.5$  s,  $t_1^1 = 2$  s,  $t_2^0 = 3$  s,  $t_2^1 = 5$  s,  $T_k^0 = T_k^1 = 0.5$  s, and  $\sigma_k = 1.3$  for  $k = 1, 2$

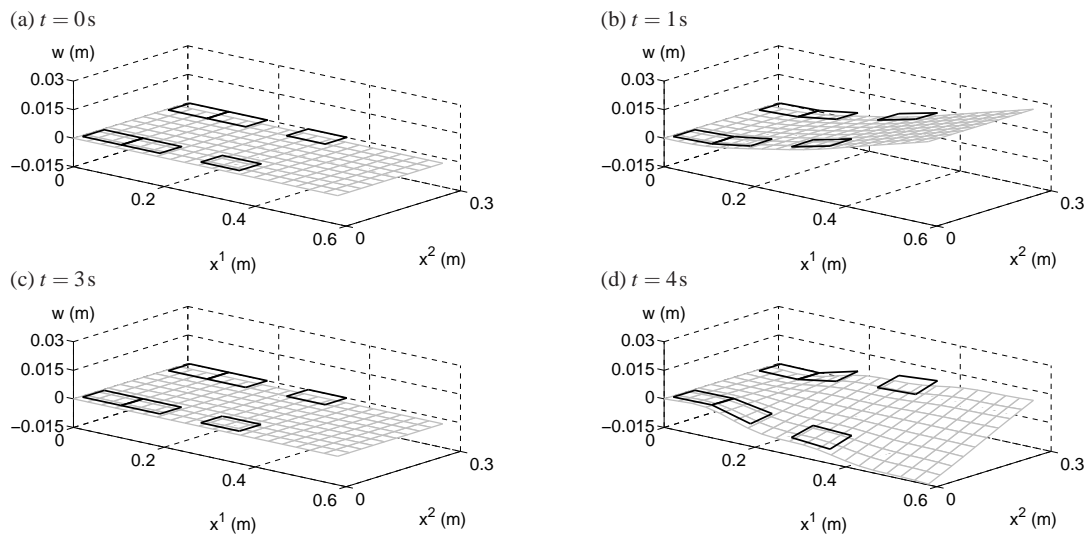


Figure 4. Plate deflection at different instances of time  $t \in \{0, 1, 3, 4\}$  s.

in order to realize a bending motion with a maximal deflection at the free corners of 0.03 m and a torsional motion with 0.015 m.

The obtained numerical results for the feedforward controlled MFC-actuated plate are presented in Fig. 4, Fig. 5 and Fig. 6. Thereby, the modal approximation (22) with  $k = 1, \dots, 20$  is used as a simulation model and is solved using a Newmark scheme. The resulting transient shaping of the rectangular plate is depicted in Fig. 4, where the plate deflection  $w(\underline{x}, t)$  as defined in (21) is shown at different instances of time  $t \in \{0, 1, 3, 4\}$  s. This clearly illustrates the desired motion consisting of a bending behavior in the first time-interval and a torsional motion in the second time-interval, also depicted in Fig. 5 (a) for three specific points at the free edge opposite the clamping  $(x^1, x^2) \in (0.6, 0), (0.6, 0.15), (0.6, 0.30)$ . The absolute tracking error in the plate domain during the first and the second time-interval, given by  $e_1 = \max_{t_0 < t < t_1 + T_1} |w(\underline{x}, t) - y^d(\underline{x}, t)|$ ,  $e_2 = \max_{t_2 < t < t_2 + T_2} |w(\underline{x}, t) - y^d(\underline{x}, t)|$ , respectively, are shown in Fig. 5 (b). Note that only the open-loop control is considered for the undamped plate model without any feedback part. The total maximal error given by  $e = \max_{\underline{x} \in \Omega} \{e_1, e_2\} = 2.1 \times 10^{-3}$  m confirms the excellent tracking performance. Furthermore, it should be pointed out that more general trajectories for the plate deflection can be realized similarly.

For the further evaluation of the tracking performance, a comparison of the desired modal states, i.e.  $w_k^d(t) = a_k(t)$ ,  $k = 1, 2$  in view of (21), (23), and (25), and the obtained modal states  $w_k(t)$ ,  $k = 1, 2$  is illustrated in Fig. 6 (a). There in addition the excitation of the residual modes  $w_k(t)$ ,  $k = 3, \dots, 20$  representing the control spillover is shown by the dotted lines. Obviously, the chosen patch configuration enables to significantly reduce the excitation of the higher order modes while ensuring that the desired trajectories  $a_k(t)$ ,  $k = 1, 2$  are tracked in an accurate way.

The corresponding input voltages  $U_q(t)$  for the  $q = 1, \dots, 6$  pairs of MFC-patches distributed according to Fig. 3, which are obtained from the evaluation of (29), are depicted in Fig. 6 (b). Note that MFC-patch actuators offer an admissible input voltage range from  $-500$  V to  $1500$  V, such that choosing the constant voltage supply  $U_0 = 500$  V the asymmetric voltage portion  $U_q(t)$  can be varied in the range of  $-1000$  V to  $1000$  V. For the chosen desired trajectory  $y^d(\underline{x}, t)$  according to (25) with coefficients (26) the two phases of bending motion and torsional motion can be clearly distinguished. In particular for the bending motion, the necessary input voltages evolve in a rather non-trivial way.

## 6. CONCLUSIONS AND FUTURE WORKS

The presented approach for flatness-based motion planning and feedforward control design for a rectangular cantilevered MFC-actuated plate modeling an adaptive airfoil is in a first step based on the analysis of an idealized scenario with infinite-dimensional input. This on the one hand allows to directly determine the state and input parametrization in terms

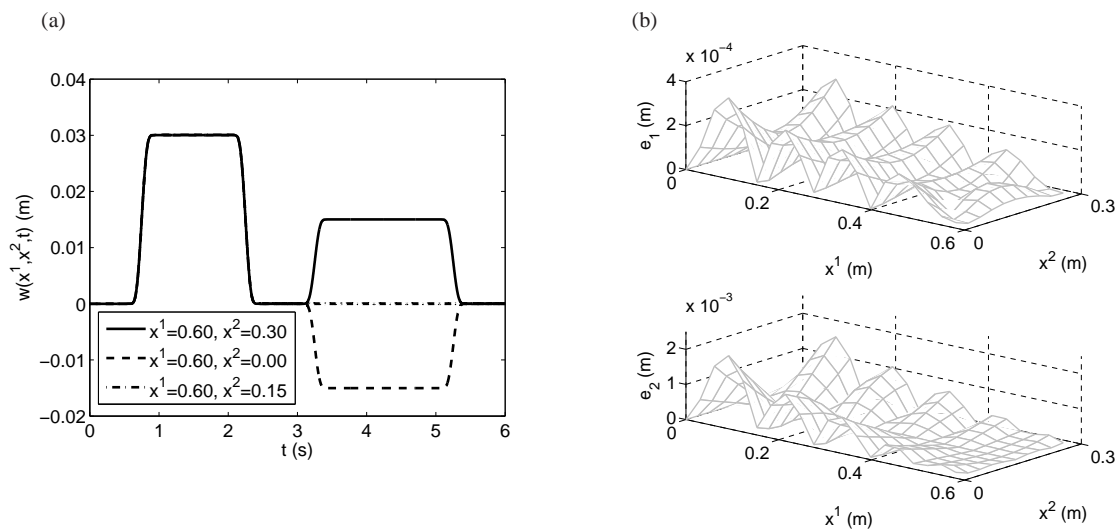


Figure 5. (a) Plate deflection at the free corners  $(x^1, x^2) = (0.6, 0)$ ,  $(x^1, x^2) = (0.6, 0.3)$  and at the middle of the free edge between the free corners  $(x^1, x^2) = (0.6, 0.15)$ . (b) Tracking error in the plate domain during the first and the second time-interval,  $e_1 = \max_{t_1^0 < t < t_1^1 + T_1^1} |w(\underline{x}, t) - y^d(\underline{x}, t)|$ ,  $e_2 = \max_{t_2^0 < t < t_2^1 + T_2^1} |w(\underline{x}, t) - y^d(\underline{x}, t)|$ , respectively.

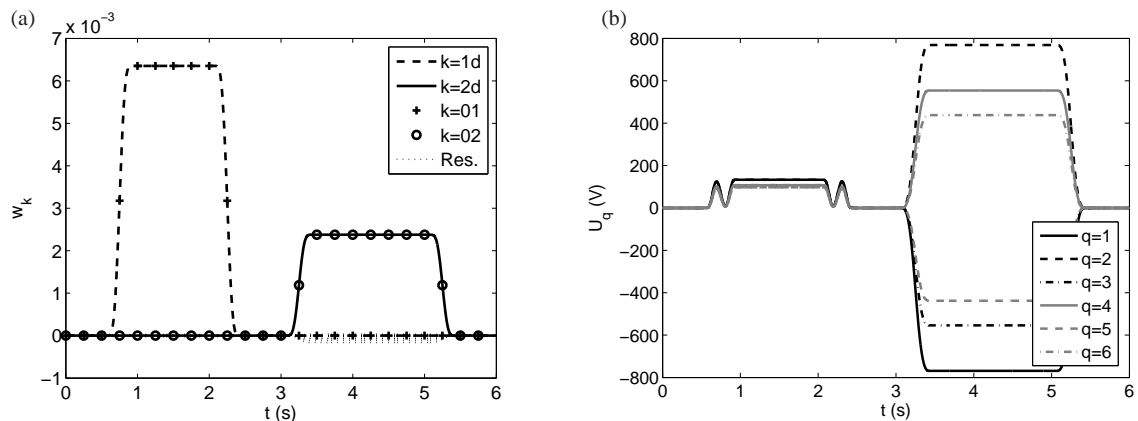


Figure 6. (a) Desired modal states  $w_k^d(t) = a_k(t)$  for  $k = 1, 2$  (indexed with  $d$  in the legend) compared to the numerically obtained states  $w_k(t)$ ,  $k = 1, 2$ , and residual states  $w_k(t)$  for  $k = 3, \dots, 20$  (dotted). (b) Input voltages  $U_q(t)$ ,  $q = 1, \dots, 6$  applied to the MFC-patches. The line styles correspond to the actuator locations shown in Fig. 3.

of the basic output and on the other hand accounts for a systematic motion planning approach. The obtained idealized input function is in a second step projected onto a finite number of suitably placed MFC-patches. For this, approaches of optimal actuator placement are used, which enable to accurately realize the inputs necessary to achieve the desired motion while suppressing control spillover. The tracking performance of the proposed approach is evaluated in a simulation scenario, where the plate is transiently deformed in order to realize a combined bending and torsional motion. However, more general trajectories can be realized similarly. In addition, the presented feedforward control will be extended by a suitable (output) feedback control, e.g., within the two-degrees-of-freedom control concept, see Ref. 15, to deal with model errors or disturbances within our future research activities.

## REFERENCES

- [1] Yousefi-Koma, A. and Zimcik, D., “Applications of Smart Structures to Aircraft for Performance Enhancement,” *Canadian Aeronautics and Space Journal* **49**(4), 163–173 (2003).
- [2] Irschik, H., “A review on static and dynamic shape control of structures by piezoelectric actuation,” *Eng. Struct.* **24**(1), 5–11 (2002).
- [3] Meurer, T. and Kugi, A., “Inversion–Based Transient Shaping of a Piezo–Actuated Plate: Motion Planning and Feedforward Control,” in [*Proc. (CD–ROM) 4th IFAC Symposium on Mechatronic Systems*], 169–174 (Sep. 12–14 2006).
- [4] Fliess, M., Mounier, H., Rouchon, P., and Rudolph, J., “Systèmes linéaires sur les opérateurs de Mikusiński et commande d’une poutre flexible,” *ESAIM Proceedings* **2**, 183–193 (1997).
- [5] Rudolph, J., [*Flatness Based Control of Distributed Parameter Systems*], Berichte aus der Steuerungs– und Regelungstechnik, Shaker–Verlag, Aachen (2003).
- [6] Meurer, T., [*Feedforward and Feedback Tracking Control of Diffusion–Convection–Reaction Systems using Summability Methods*], Fortschr.–Ber. VDI Reihe 8 Nr. 1081, VDI Verlag, Düsseldorf (2005).
- [7] “Smart Material Corp.” <http://www.smart-material.com>.
- [8] Nowacki, W., [*Dynamic Problems of Thermoelasticity*], Noordhoff Int. Publ., PWN–Polish Scientific Publ., Warszawa (1975).
- [9] Meirovitch, L., [*Principles and Techniques of Vibrations*], Prentice Hall, New Jersey (1997).
- [10] Banks, H., Smith, R., and Wang, Y., [*Smart Material Structures: Modeling, Estimation and Control*], John Wiley & Sons (1996).
- [11] Curtain, R. and Zwart, H., [*An Introduction to Infinite–Dimensional Linear Systems Theory*], Texts in Applied Mathematics 21, Springer–Verlag, New York (1995).
- [12] Reddy, J., [*Theory and Analysis of Elastic Plates*], Taylor & Francis (1984).
- [13] Gawronski, W., [*Dynamics and Control of Structures*], Springer–Verlag, New York (1998).
- [14] Halim, D. and Moheimani, S., “An optimization approach to optimal placement of collocated piezoelectric actuators and sensors on a thin plate,” *Mechatronics* **13**, 27–47 (2003).
- [15] Meurer, T., Thull, D., and Kugi, A., “Flatness–based tracking control of a piezoactuated Euler–Bernoulli beam with non–collocated output feedback: theory and experiments,” *Int. J. Control* **81**(3), 473–491 (2008).